One-arm spiral instability in hypermassive neutron stars formed by dynamical-capture binary neutron star mergers

Vasileios Paschalidis, William E. East, Frans Pretorius, and Stuart L. Shapiro

Phys. Rev. D **92**, 121502 — Published 30 December 2015

DOI: 10.1103/PhysRevD.92.121502

One-arm Spiral Instability in Hypermassive Neutron Stars Formed by Dynamical-Capture Binary Neutron Star Mergers

Vasileios Paschalidis[1], William E. East[2], Frans Pretorius[1], and Stuart L. Shapiro[3,4]
[1]*Department of Physics, Princeton University, Princeton, NJ 08544, USA*
[2]*Kavli Institute for Particle Astrophysics and Cosmology, Stanford University, SLAC National Accelerator Laboratory, Menlo Park, CA 94025, USA*
[3]*Department of Physics, University of Illinois at Urbana-Champaign, Urbana, IL 61801*
[4]*Department of Astronomy & NCSA, University of Illinois at Urbana-Champaign, Urbana, IL 6180*

Using general-relativistic hydrodynamical simulations, we show that merging binary neutron stars can form hypermassive neutrons stars that undergo the one-arm spiral instability. We study the particular case of a dynamical capture merger where the stars have a small spin, as may arise in globular clusters, and focus on an equal-mass scenario where the spins are aligned with the orbital angular momentum. We find that this instability develops when post-merger fluid vortices lead to the generation of a toroidal remnant — a configuration whose maximum density occurs in a ring around the center-of-mass — with high vorticity along its rotation axis. The instability quickly saturates on a timescale of ~ 10 ms, with the $m = 1$ azimuthal density multipole mode dominating over higher modes. The instability also leaves a characteristic imprint on the post-merger gravitational wave signal that could be detectable if the instability persists in long-lived remnants.

PACS numbers: 04.25.D-,04.25.dk,04.30.-w

Introduction.—The possibility of observing the inspiral and merger of neutron star–neutron star (NSNS) binaries is an exciting prospect that soon may be realized. Often referred to as "multimessenger" sources, NSNSs emit copious amounts of gravitational waves (GWs), and hence are a primary target of ground-based laser interferometers such as aLIGO [1], VIRGO [2] and KAGRA [3], and may generate transient electromagnetic (EM) signals, both before [4–8] and after [9, 10] merger. These EM transients could be observed by current and future telescopes, such as PTF [11], PanSTARRS [12], and LSST [13]. By combining GW and EM signals from NSNSs one can in principle test relativistic gravity and constrain the behavior of matter at super-nuclear densities. Furthermore, NSNS mergers may offer explanations to long-standing astrophysical puzzles, such as the nature of short-hard gamma ray burst progenitors [14–16], and the origin of r-process elements [17].

The interpretation of EM and GW signals from NSNS mergers will rely on a solid theoretical understanding of these events. Such understanding requires simulations in full general relativity (GR) to treat both the rapidly varying, strong field spacetime and the relativistic velocities that naturally arise in these events. There have been numerous such studies, mostly focusing on quasi-circular inspiral and mergers (see, e.g. [18] for a review, and [19–24] for recent work), but also some simulations of eccentric inspiral and mergers [25, 26]. The latter binaries may be dynamically assembled in dense stellar systems such as globular clusters (GCs) through single-single [27, 28] or binary-single star interactions [29]. Although the rates are very uncertain, they have been estimated to be as high as $\sim 50\ \mathrm{yr}^{-1}\ \mathrm{Gpc}^{-3}$ [28]. Note though that the majority of events sourced by binary-single interactions will enter the aLIGO frequency band ($\gtrsim 10$ Hz) as low eccentricity systems. Also, though a recent study of dynamically assembled hierarchical triple systems in GCs found Lidov-Kozai induced merger of the inner binary could lead optimistically to several aLIGO detections per year of highly eccentric *black hole* binaries, they estimated that this channel would offer a negligible contribution to NSNS merger rates [30]. Another aspect of NSNS systems dynamically assembled in GCs important to the work presented here is that (regardless of eccentricity at merger) the individual NSs are likely to have non-negligible spin, given the large population of millisecond pulsars (MSPs) found there (see [31] for further discussion on the relevance of NS spin in compact binaries).

A NSNS merger may not immediately form a black hole (BH), but instead result in a hypermassive NS (HMNS)—a long-lived, but transient remnant that is supported against collapse by differential rotation and thermal energy. Here we report results from a simulation where a HMNS forms after the eccentric merger of two equal mass NSs that each have a spin period of 10.6 ms. An important feature we discover is that the HMNS develops the so-called one-arm ($m = 1$) spiral instability. This instability grows from seeds at the level of numerical truncation error to dominate eventually the azimuthal perturbations of the star. In a follow-up work [32] we will present results from a broader range of initial conditions, in particular asymmetric cases where the initial data does contain a small $m = 1$ component, suggesting that our results are robust and not at artifact of truncation error. Since the qualitative features of the instability do not seem to depend on how we seed the initial mode, here we restrict discussion to this one case.

The one-arm instability was first seen in Newtonian simulations of differentially rotating stars with soft equations of state (EOSs) [33], and argued to be triggered by a toroidal structure in the stellar density profile [34]. Motivated by [35], [36] suggested that this instability develops near the corotation radius of the HMNS, i.e. where the azimuthal pattern speed of the unstable mode is commensurate with the local angular velocity of fluid elements of the star. Newtonian [37] and general-relativistic [38] simulations of isolated rotating stars seem to confirm this interpretation. The one-arm spiral instability can develop in isolated stars even for stiff equations of state [37], and has been found to occur in proto-NSs formed in Newtonian [39] and general-relativistic [40, 41] core-collapse simulations. Although it has been speculated that it could operate in the HMNS remnants of NSNS mergers [34], the one-arm spiral instability has not been reported to occur in NSNS mergers until now. Here we demonstrate using GR hydrodynamic simulations that the instability can develop in a NSNS dynamical capture merger remnant, and offer a description of how the process unfolds in terms of post-merger vortex dynamics. We also show that the mode produces a strong $m = 1$ component to the GW signal, which, if sufficiently long-lived, could be observable by aLIGO.

Methodology.—Our simulations are performed using the code described in [42]. The Einstein field equations are solved in the generalized-harmonic formulation using finite difference methods, while the matter is modeled as a perfect fluid with the corresponding hydrodynamic equations evolved using high-resolution shock-capturing techniques described in [43].

We prepare constraint-satisfying initial data as in [26, 44], except that here the data (matter and velocity profiles, and freely specifiable fields) are a superposition of two rigidly-rotating, equilibrium NSs, generated with the code of [45, 46]. Each of the stars has a mass of 1.35 $M_\odot$ and dimensionless spin $J_{\rm NS}/M_{\rm NS}^2 = 0.05$ (we adopt geometrized units with $G = c = 1$ throughout unless otherwise specified) aligned with the ortital angular momentum. The initial separation is $d = 50M \simeq 200$ km [where M is the total Arnowit-Deser-Misner (ADM) mass] and the velocities and positions of the stars correspond to a marginally unbound Newtonian orbit of periapse $r_p = 8M$. We adopt the "HB" piece-wise polytropic cold EOS of [47] for the matter, which yields a maximum static mass of 2.12 $M_\odot$ (2.53 $M_\odot$ allowing for maximal uniform rotation). For the evolution we incorporate a thermal component to the EOS, $P_{\rm th} = 0.5\epsilon_{\rm th}\rho_0$, to allow for shock-heating. Here, $\epsilon_{\rm th}$ is the thermal component of the specific internal energy ϵ, and ρ_0 is the rest mass density.

We employ adaptive mesh refinement (AMR), where our hierarchy consists of six levels that are dynamically adjusted during the evolution based on metric truncation-error estimates. For convergence studies we

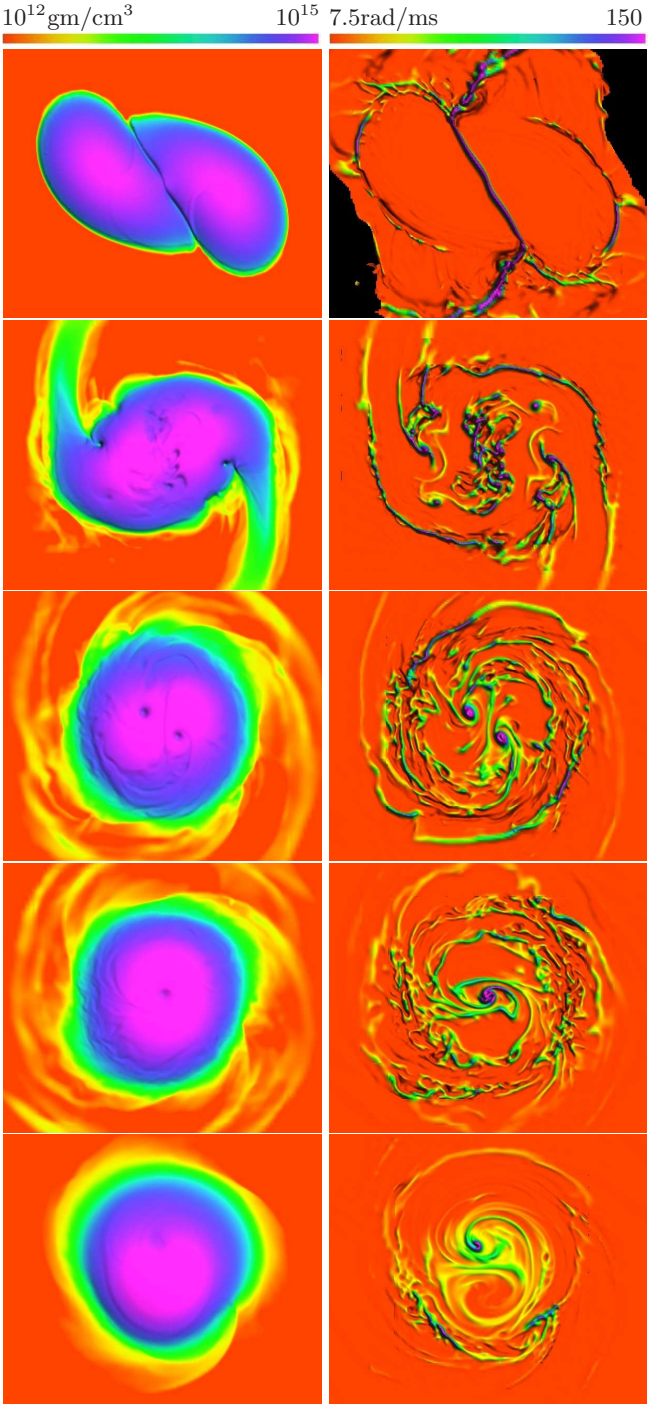

FIG. 1. Equatorial rest-mass density (left) and Ω_{xy} (right) snapshots at select times, advancing from top to bottom. At $t \approx 3.1$ ms the NSs collide, leading to a vortex sheet. A couple of rotation periods later at $t \approx 4.5$ ms two larger vortices form near the surface of the star at the shearing layers between the surface and the tidal tails. These two vortices inspiral toward the center ($t \approx 5.5$ ms) and merge ($t \approx 6.5$ ms) creating an underdense center. This near-stationary, near-axisymmetric configuration persists for a few milliseconds, though the one-arm instability is now growing, eventually expelling the central vortex and associated underdensity from the center. By $t \approx 14.6$ ms the instability is fully developed. Each panel is ≈ 50 km per side.

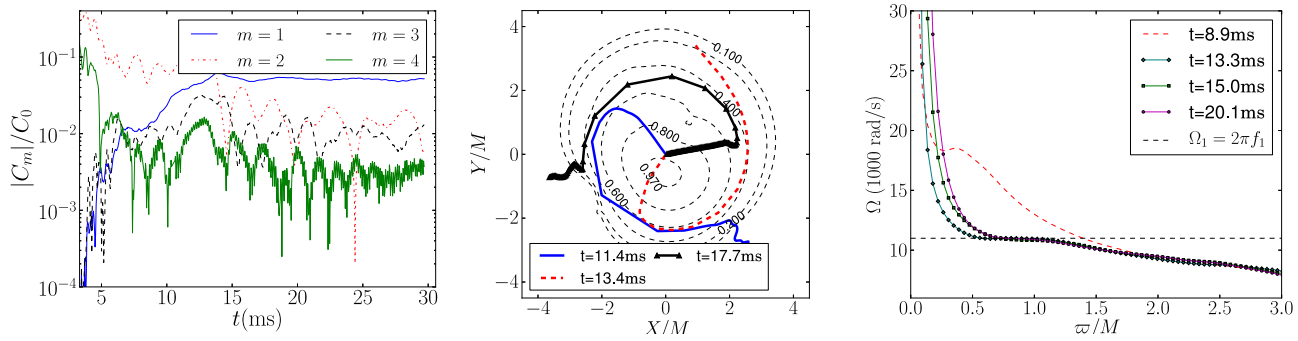

FIG. 2. Left: The magnitude of C_m normalized to C_0. Middle: The thick lines illustrate the phase of the mode C_1 as a function of radius ϖ (specifically, we plot $X + iY = \varpi C_1(\varpi, 0)/|C_1(\varpi, 0)|$) at select times. Dashed thin lines are contours of ρ_0 at $t = 13.4$ ms, normalized to its maximum value then. The inlined numbers label the values of the level surfaces. The tiny contour at $X/M \approx Y/M \approx 1$ corresponds to a value of 0.6 and is at the location of the vortex. Right: azimuthally averaged angular velocity at select times. Here $M = 2.7M_\odot \simeq 3.99$ km. Merger occurs at $t \simeq 3.0$ ms.

perform the simulations using three resolutions. All figures use data from the highest resolution run, which has a base-level grid of 321^3 points and a finest level covering the eventual HMNS diameter with ~ 200 points. The low and medium resolution runs have 2 and 1.5625× the grid spacing, respectively.

To analyze the one-arm spiral instability we use several diagnostics. We compute the azimuthal mode decomposition of the conserved rest-mass density $C_m(\varpi, z) = \frac{1}{2\pi}\int_0^{2\pi} \rho_0 u^0 \sqrt{-g} e^{im\phi} d\phi$, where $\varpi = \sqrt{x^2+y^2}$ is the cylindrical coordinate radius, ϕ is the azimuthal angle, u^μ is the fluid 4-velocity, and g the determinant of the spacetime metric. A similar quantity integrated throughout the star is $C_m = \int \rho_0 u^0 \sqrt{-g} e^{im\phi} d^3x$. We follow the xy-component of the vorticity 2-form $\Omega_{\mu\nu} = \nabla_\mu(hu_\nu) - \nabla_\nu(hu_\mu)$ on the equatorial plane, where ∇_μ is the covariant derivative, and $h = 1 + \epsilon + P/\rho_0$ the specific enthalpy, with P the pressure. We also compute the ratios of total kinetic ($T_{\rm kin}$) and rotational kinetic energy ($T_{\rm rot}$) to the gravitational potential energy $|W|$ as in [45, 46, 48, 49], but in a coordinate center-of-mass frame: $x^i_{\rm cm} = \frac{1}{C_0}\int x^i \rho_0 u^0 \sqrt{-g} d^3x$. These diagnostics are not gauge independent, but are nevertheless useful in identifying qualitative features of the one-arm spiral instability.

Results.—Following merger we find a long-lived HMNS that is subject to the one-armed spiral instability. In Fig. 1 we show equatorial ρ_0 and Ω_{xy} snapshots illustrating the dynamics. Two larger vortices form near the surface of the HMNS from shearing with the tidal tails, and subsequently spiral towards the center and merge, creating an underdensity around the rotation axis. (Numerous other smaller vortices also form during the early stage of the merger, in particular interior to the HMNS following break-up of the vortex sheet formed at first contact, but for the most part they are quickly stretched away and do not seem to play a significant role in creating the underdense core.) The one-arm spiral instability is triggered around this time, in agreement with earlier Newtonian simulations [34] which suggest that such a toroidal HMNS configuration is a necessary condition for the instability. This is consistent with the growth of the C_1 mode shown in the left panel of Fig. 2. Several milliseconds after formation of the underdense core, ~ 11 ms after merger, C_1 has grown to saturation, dominating the azimuthal modes of the HMNS. We can characterize the approximate growth rate of the instability by noting that it takes ≈ 1.2 ms for this mode to grow from 1/4 to 1/2 its saturation level. From the Fourier transform of C_m we determine the dominant frequencies f_m of the density modes to be $f_1 = 1.75$ kHz, $f_2 = 3.4$ kHz, and $f_3 = 5.2$ kHz, i.e., $f_m \approx m \times f_1$. The time to saturation and frequency of the $m = 1$ mode differ by at most 15% and 2% among the different resolutions, respectively. We find that the time to saturation (saturation amplitude) decreases (increases) with resolution.

The characteristic one-arm spiral pattern of the instability can be seen in the middle panel of Fig. 2, which shows the phase of the $m = 1$ mode in the equatorial plain. The right panel in Fig. 2 plots the azimuthally averaged angular velocity of the fluid in the HMNS as a function of radius at several times. If we take the angular frequency $2\pi f_1$ (horizontal line in the panel) calculated above from the time dependence of C_1 to be the oscillation frequency of the unstable mode, the right panel shows that there exists a corotation radius at $\varpi \approx 1.4$M prior to the development of the instability. Following saturation of the instability, the region $0.5M \lesssim \varpi \lesssim 1.2M$ rotates almost rigidly with this same angular frequency.

After the HMNS settles from the violence of the merger (by $t \simeq 7$ ms), we find $T_{\rm kin}/|W| \approx T_{\rm rot}/|W| \approx 0.26$, and steadily drops to 0.23 as the instability saturates. Thus,

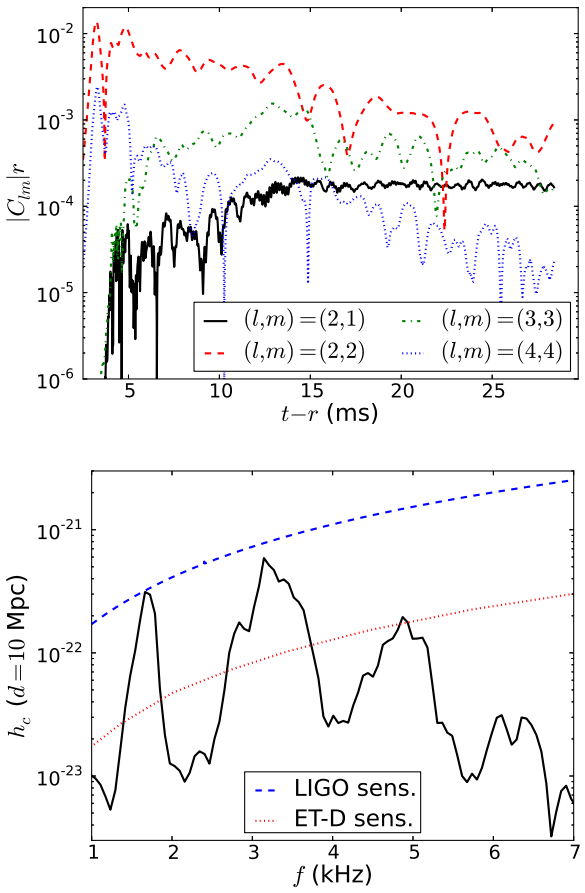

FIG. 3. Top: the amplitude of spin-weight -2 spherical harmonic components of the post-merger GW signal. Bottom: the full GW spectrum from the last $\sim$ 15 ms (when the instability is fully developed), as would be seen by an edge-on observer 10 Mpc away. Also plotted are the aLIGO and proposed Einstein Telescope (ET-D) sensitivity curves [51]. If the $m = 1$ mode persists as long as the HMNS lifetime $t_{\rm HMNS}$, estimated to be $\sim O(1)$ s, the peak power at ~ 1.7 kHz could be enhanced by a factor $t_{\rm HMNS}/(15\ {\rm ms}) \sim O(10^2)$. Thus, if the event takes place nearby within 10 Mpc, then it could be detectable by aLIGO.

to within gauge ambiguities, the instability cannot be classified as a low-$T/|W|$ instability, but $T/|W|$ is slightly below the usual threshold for the dynamical bar mode instability [50].

The upper panel of Fig. 3 shows the leading spherical harmonic components of the post-merger GW signal. The $(\ell, m) = (2, 1)$ mode mirrors the growth and saturation of the C_1 density perturbation, but remains sub-dominant compared to the $(\ell, m) = (2, 2)$ and $(\ell, m) = (3, 3)$ over the time simulated. However, in terms of detectability as the GW power spectrum shown in the lower panel of Fig. 3 indicates, the less GW power in the $m = 1$ mode is in part offset by the lower frequency of the mode where ground-based detectors have greater sensitivity.

Comparison with the aLIGO sensitivity curve in Fig. 3 shows the part of the GW signal due to the one-arm instability is too weak for likely detection, unless the HMNS and excited $m = 1$ mode can persist for a time considerably longer than the length of the simulation. From Figs. 2 and 3 we note that after saturation the $m = 1$ mode and corresponding GW signal persists at roughly constant amplitude till the end of the simulation, in contrast to the other modes that trend to decay. Thus, the $m = 1$ component of the signal may last much longer than the ≈ 15 ms of integration used in Figs. 3, possibly even the entire lifetime of the HMNS before collapse to a BH. A rough estimate of this lifetime calculated from the rate of angular momentum loss to GWs and amount of unradiated angular momentum at the end of the simulation gives $t_{\rm HMNS} = J_{\rm ADM}/\dot{J}_{\rm GW} \sim 2$ s, which could give an additional factor of $O(10^2)$ in GW power and make the mode detectable by aLIGO out to ≈ 10 Mpc and by the ET out to ≈ 100 Mpc. However, as angular momentum is lost to gravitational radiation, the frequency of the mode may not remain constant, and hence the peak power of the mode will not increase with time as that for a near-monochromatic source. Longer high-resolution simulations are necessary to study this effect.

Concluding Remarks.—First, some caveats related to the numerics are in order. Though we do see the expected second-order convergence for the pre-merger epoch, our resolution sequence is not high enough to show the expected first-order (due to shocks) convergence for the post-merger epoch in certain quantities. This is likely because with higher resolution we observe the appearance of ever smaller scale vortices following merger, and it is very challenging to achieve convergence in such a turbulent-like environment. However, essential qualitative features of the post-merger remnant appear robust, most importantly, the development of the one-arm instability and its order-of-magnitude growth time, frequency and saturation amplitude. On the other hand, our low resolution run forms a BH $\sim$ 19 ms following merger, whereas the medium and high resolution have not, even after the $\sim$ 27 ms they were continued post merger. This suggests our order of magnitude estimate above for the lifetime of the HMNS may be too optimistic. However, there are many factors that will affect the actual lifetime of a HMNS, including physical effects we do not model (e.g. magnetic fields and neutrino cooling), parameters quantifying uncertainty in the EOS (for stiff EOSs typical HMNS remnants may possibly survive for $\sim 2-3$ s [52]), and the broader range of relevant initial conditions (e.g. mass ratio, lower eccentricity at merger, spin orientation). Conversely, strong sensitivity of the lifetime of the HMNS to properties of the system means greater possibility of measuring related quantities from putative future multi-messenger observations.

More details on convergence, other cases, and other

properties of these mergers will be presented in [32]. Important questions for future work are what elements of the particular case studied here are essential to give rise to the instability, and why it was not present and/or pointed out in previous studies. It could be that only some combination of orbital eccentricities, a particular EOS, component masses and spins lead to a long-lived, unstable HMNS. Alternatively, these factors could affect the growth rate such that the structure of the instability was not clearly seen by the termination of earlier simulations. For example, [53] reported strong $m = 1$ modes in HMNS remnants from quasicircular NSNS mergers with spinning NSs (employing a Γ-Law EOS and initial 1.5 $M_\odot$ NSs), though there they were ascribed as likely due to "mode couplings". The $t > 100$ ms post-merger evolution of a HMNS presented in [54] would not have seen any odd-m instabilities due to the π symmetry enforced there. It is important to resolve these issues for quasicircular mergers involving spinning NSs, for as discussed in the introduction, these are the most likely sources of observable GWs from dynamically assembled systems in GCs. We plan to address many of these issues in future work.

It is a pleasure to thank Tom Abel, Andreas Bauswein, and Roman Gold for useful discussions. This work was supported by the Simons Foundation and NSF grant PHY-1305682 at Princeton University, as well as NSF grant PHY-1300903 and NASA grant NNX13AH44G at the University of Illinois at Urbana-Champaign. Computational resources were provided by XSEDE/TACC under grants TG-PHY100053, TG-MCA99S008, and the Orbital cluster at Princeton University.

[1] A. Abramovici et al., Science **256**, 325 (1992).
[2] B. Caron *et al.*, Class. Quant. Grav. **14**, 1461 (1997).
[3] LCGT Collaboration, K. Somiya, Class.Quant.Grav. **29**, 124007 (2012), 1111.7185.
[4] B. M. Hansen and M. Lyutikov, Mon.Not.Roy.Astron.Soc. **322**, 695 (2001), astro-ph/0003218.
[5] S. T. McWilliams and J. Levin, Astrophys. J.**742**, 90 (2011), 1101.1969.
[6] V. Paschalidis, Z. B. Etienne, and S. L. Shapiro, Phys.Rev. **D88**, 021504 (2013).
[7] C. Palenzuela *et al.*, Physical Review Letters **111**, 061105 (2013), 1301.7074.
[8] M. Ponce, C. Palenzuela, L. Lehner, and S. L. Liebling, Phys. Rev. D**90**, 044007 (2014), 1404.0692.
[9] B. D. Metzger and E. Berger, Astrophys. J.**746**, 48 (2012), 1108.6056.
[10] B. D. Metzger, A. Bauswein, S. Goriely, and D. Kasen, Mon. Not. Roy. Astron. Soc.**446**, 1115 (2015), 1409.0544.
[11] A. e. a. Rau, PASP **121**, 1334 (2009), 0906.5355.
[12] N. Kaiser *et al.*, Pan-STARRS: A Large Synoptic Survey Telescope Array, in *Survey and Other Telescope Technologies and Discoveries*, edited by J. A. Tyson and S. Wolff, , Society of Photo-Optical Instrumentation Engineers (SPIE) Conference Series Vol. 4836, pp. 154–164, 2002.
[13] LSST Dark Energy Science Collaboration, ArXiv e-prints (2012), 1211.0310.
[14] T. Piran, Reviews of Modern Physics **76**, 1143 (2005).
[15] P. Meszaros, Rept.Prog.Phys. **69**, 2259 (2006).
[16] V. Paschalidis, M. Ruiz, and S. L. Shapiro, Astrophys. J. Lett.**806**, L14 (2015), 1410.7392.
[17] S. Rosswog, F. K. Thielemann, M. B. Davies, W. Benz, and T. Piran, Coalescing Neutron Stars: a Solution to the R-Process Problem?, in *Nuclear Astrophysics*, edited by W. Hillebrandt and E. Muller, p. 103, 1998, arXiv:astro-ph/9804332.
[18] J. A. Faber and F. A. Rasio, ArXiv e-prints (2012), 1204.3858.
[19] V. Paschalidis, Z. B. Etienne, and S. L. Shapiro, Phys. Rev. D**86**, 064032 (2012), 1208.5487.
[20] D. Neilsen *et al.*, Phys. Rev. D**89**, 104029 (2014), 1403.3680.
[21] K. Dionysopoulou, D. Alic, and L. Rezzolla, ArXiv e-prints (2015), 1502.02021.
[22] Y. Sekiguchi, K. Kiuchi, K. Kyutoku, and M. Shibata, Phys. Rev. D**91**, 064059 (2015), 1502.06660.
[23] T. Dietrich, S. Bernuzzi, M. Ujevic, and B. Bruegmann, ArXiv e-prints (2015), 1504.01266.
[24] C. Palenzuela *et al.*, ArXiv e-prints (2015), 1505.01607.
[25] R. Gold, S. Bernuzzi, M. Thierfelder, B. Bruegmann, and F. Pretorius, ArXiv e-prints (2011), 1109.5128.
[26] W. E. East and F. Pretorius, Astrophys. J. Lett.**760**, L4 (2012), 1208.5279.
[27] B. Kocsis and J. Levin, Phys. Rev. D**85**, 123005 (2012), 1109.4170.
[28] W. H. Lee, E. Ramirez-Ruiz, and G. van de Ven, Astrophys. J.**720**, 953 (2010), 0909.2884.
[29] J. Samsing, M. MacLeod, and E. Ramirez-Ruiz, Astrophys.J. **784**, 71 (2014), 1308.2964.
[30] F. Antonini *et al.*, ArXiv e-prints (2015), 1509.05080.
[31] W. E. East, V. Paschalidis, and F. Pretorius, Astrophys. J. Lett.**807**, L3 (2015), 1503.07171.
[32] W. E. East, V. Paschalidis, F. Pretorius, and S. L. Shapiro, in preparation (2015).
[33] J. M. Centrella, K. C. B. New, L. L. Lowe, and J. D. Brown, Astrophys. J. Lett.**550**, L193 (2001), astro-ph/0010574.
[34] M. Saijo, T. W. Baumgarte, and S. L. Shapiro, Astrophys. J.**595**, 352 (2003), astro-ph/0302436.
[35] A. L. Watts, N. Andersson, and D. I. Jones, Astrophys. J. Lett.**618**, L37 (2005), astro-ph/0309554.
[36] M. Saijo and S. Yoshida, Mon. Not. Roy. Astron. Soc.**368**, 1429 (2006), astro-ph/0505543.
[37] S. Ou and J. E. Tohline, Astrophys. J.**651**, 1068 (2006), astro-ph/0604099.
[38] G. Corvino, L. Rezzolla, S. Bernuzzi, R. De Pietri, and B. Giacomazzo, Classical and Quantum Gravity **27**, 114104 (2010), 1001.5281.
[39] C. D. Ott, S. Ou, J. E. Tohline, and A. Burrows, Astrophys. J. Lett.**625**, L119 (2005), astro-ph/0503187.
[40] C. D. Ott *et al.*, Physical Review Letters **98**, 261101 (2007), astro-ph/0609819.
[41] T. Kuroda, T. Takiwaki, and K. Kotake, Phys. Rev. D**89**, 044011 (2014), 1304.4372.
[42] W. E. East, F. Pretorius, and B. C. Stephens, Phys. Rev. D **85**, 124010 (2012).

[43] W. E. East, F. Pretorius, and B. C. Stephens, Phys. Rev. D **85**, 124009 (2012).
[44] W. E. East, F. M. Ramazanoglu, and F. Pretorius, Phys.Rev. **D86**, 104053 (2012), 1208.3473.
[45] G. B. Cook, S. L. Shapiro, and S. A. Teukolsky, Astrophys. J.**424**, 823 (1994).
[46] G. B. Cook, S. L. Shapiro, and S. A. Teukolsky, Astrophys. J.**422**, 227 (1994).
[47] J. S. Read *et al.*, Phys. Rev. D**79**, 124033 (2009), 0901.3258.
[48] T. W. Baumgarte and S. L. Shapiro, *Numerical Relativity: Solving Einstein's Equations on the Computer* (, 2010).
[49] K. Kiuchi, K. Kyutoku, and M. Shibata, Phys. Rev. D**86**, 064008 (2012), 1207.6444.
[50] M. Shibata, T. W. Baumgarte, and S. L. Shapiro, Astrophys. J.**542**, 453 (2000), astro-ph/0005378.
[51] S. Hild *et al.*, Classical and Quantum Gravity **28**, 094013 (2011), 1012.0908.
[52] Y. Sekiguchi, K. Kiuchi, K. Kyutoku, and M. Shibata, Phys. Rev. Lett. **107**, 051102 (2011).
[53] S. Bernuzzi, T. Dietrich, W. Tichy, and B. Bruegmann, Phys.Rev. **D89**, 104021 (2014), 1311.4443.
[54] L. Rezzolla, L. Baiotti, B. Giacomazzo, D. Link, and J. A. Font, Classical and Quantum Gravity **27**, 114105 (2010), 1001.3074.